Supporting Information **(SI)** *for*

Metal-organic frameworks supported on nanofibers to remove heavy metals

Johnson E. Efome, Dipak Rana*, Takeshi Matsuura, Christopher Q. Lan

Industrial Membrane Research Institute, Department of Chemical and Biochemical Engineering, University of Ottawa, 161 Louis Pasteur Ottawa, ON K1N 6N5, Canada

Table of Contents

Experimental section....2

Synthesis of MOF 808....2

Batch adsorption-desorption experiments....3

Filtration experiment....5

Instrumentations....5

References....7

List of figures....9

List of tables....10

Experimental section

All chemicals were of analytical grade, commercially available from Sigma Aldrich, Alfa Aesar and Strem chemical, and used as received without further purification.

Synthesis of MOF 808

The crystals were synthesized by facile microwave procedure[1], with a modified route from Furukawa et al.[2]. Typically, 0.699 g of $ZrCl_4$ and H_3BTC (0.210 g) were dissolved in a mixture of N,N-dimethyl formamide (DMF)/Formic acid (45/45 mL) in a 200 mL boiling flask. The flask was then transferred into a microwave and irradiated at 400 W for 30 min. The resulting suspension was filtered by centrifugation, washed with DMF three times (10 x 3) and dried at 70^{o}C for 12 h. Solvent exchange in acetone and water followed by vacuum drying at 50^{o}C was also done as an activation route.

MOF F300

This was a commercially purchased MOF from Sigma Aldrich Co., St. Louis, MO, produced by BASF, Germany and marketed under the name Basolite F300 (CAS # 1195763-37-1, Mw = 262.96 Da) and also known as Fe-BTC, Iron 1,3,5-Benzenetricarboxylate (BTC). The manufacturer reported it has a BET (Brunauer, Emmett and Teller) surface area of 1300-1600 m^2/g, and bulk density of 0.16-0.35 g/cm^3.

Preparation of electrospinning solution:

PAN solution: 0.5 g of PAN (average Mw = 150 kDa, and density of 1.184 g/cm^3 from Sigma Aldrich Co., St. Louis, MO) was added to 5 g of DMF and the solution was placed in a shaker (180 rpm) for 24 h at 50^{o}C to form a homogenous 10 wt% solution.

PVDF solution: 1.0 g of PVDF (Mw = 410 kDa; melt viscosity 18.5 ± 2.5 kPoise; melting temperature, Tm 160.1^{o}C, Kynar® 740 Pellet from Arkema Inc., Philadelphia, PA) pellets was added to 5 mL of DMF and the mixture stirred overnight (under same temperature and rpm as above) to form a 20 w/v homogeneous solution.

Preparation of MOF/polymer dope solution: 0.125 g of MOF was primed in 3 g of DMF. Then 0.5 g of PAN was added with the remainder of 2 g solvent to form a suspension with 20 wt% MOF

loading. For PVDF, since the viscosity was optimized, MOF loading was kept at a maximum of 16 wt%.

Preparation of nanofiber membranes and NMOM:

Neat membranes

The 10 wt% PAN/DMF solution was filled into a 10-mL syringe and electrospun at a syringe feed rate of 0.15mm/min. A voltage of 15 kV was applied to a spinneret of 0.6 mm ID separated from a 140 rpm rotating drum 15 cm apart. The temperature and humidity were maintained at 25^{o}C and 40%, respectively. The nonwoven fibers were collected on aluminium foil and dried at room temperature for 24 h. The 20 w/v PVDF/DMF solution was electrospun at a voltage of 18 kV, syringe feed rate of 0.1 mm/min, and a spinneret collector drum distance of 15 cm.

MOF/PAN nanofibers

The dope solution was electrospun on aluminium foil at 15-17 kV, 0.15 mm/min syringe feed rate and under the same temperature and humidity as above.

MOF/PVDF nanofibers

Fibers were also collected on aluminium foil under an applied voltage of 18-20 kV, 0.10-0.12 mm/min syringe feed rate and 15 cm drum-spinneret distance.

Batch adsorption-desorption experiments

The synthetic lead and mercury solution were made by dissolving lead(II) nitrate and mercury(II) chloride, respectively (From Strem chemicals), in distilled water and were further diluted to the required concentrations. All sample concentrations were measured using flame atomic absorption spectroscopy (FAAS). To determine the amount of heavy metal adsorbed to MOFs, the difference in concentrations between before and after adsorption was computed. To reuse membranes after each cycle, the adsorbates, heavy metals, were desorbed from NMOM. Desorption experiments were carried out using 2 wt% nitric acid solution. Since heavy metals precipitation turns to occur at pH >5, all experiments were conducted below pH 5 i.e., pH 4.6 ± 0.2 adjusted using 0.1 M HCl or 0.1 M NaOH.

Adsorption kinetics experiments were performed to determine adsorption rate and the time for the MOF to reach the adsorption equilibrium. Twenty milligram (20 mg) of M808 and 10 mg of F300 were used in separate experiments with 30 mL of 20 ppm lead, and 50 ppm of mercury initial concentration. The samples, collected at predetermined time intervals, were agitated slowly at room temperature for a total contact time of 3 h.

The adsorption isotherms of the MOF were established by using the same masses of the MOFs as above but with different initial heavy metal concentrations; Lead (10-1000 ppm), mercury (50-1000 ppm). From the results of kinetics experiments, 2 h was sufficient for equilibrium to be attained. The membrane isotherms were established by weighing specific mass of the membrane (with and without MOF) ranging between 50-70 mg and using the same concentrations and volumes of the heavy metal solutions. The pH was maintained at 4.6±0.2 by using nitric acid/sodium hydroxide and the temperature was kept at room temperature. The bound heavy metal was desorbed by soaking the membrane in 30 mL of diluted nitric acid, to decrease the pH and change the surface charge, under mild agitation for 1 h at room temperature.

The amount of adsorbate adsorbed per unit mass of adsorbent q_e (mg g^{-1}) and the distribution coefficient[3] (mass-weighted coefficient representing the sorbent's affinity for a sorbate: K_d) are given by equations (1) and (2), respectively.

$$q_e = \frac{(Co - Ce)\,V}{m} \tag{1}$$

$$K_d = \frac{Co - Ce}{Ce} * \frac{V}{m} \tag{2}$$

where m (g) is the mass of adsorbent, V(L) is the volume of the solution, C_o and C_e are the initial and equilibrium concentrations (mg L^{-1}). K_d values were determined using a 2 ppm solution of the heavy metal ion with the same volume and mass of sorbent as in the kinetics analysis.

To calculate the percent of MOF available for adsorption, when enmeshed and not enmeshed:

$$q_{max}^{NMOM} = q_{max}^{NFM} * (\%NFM) + q_{max}^{MOF} * (\%MOF) \tag{3}$$

where the superscript NFM is the nanofiber mat, NMOM is the nanofiber MOF membrane, MOF is the metal-organic framework, q_{max} is the maximum adsorption capacities of the respective sorbent.

Filtration experiment

Filtration experiments were conducted using a dead-end cell of 300 mL volume capacity and an effective membrane area of 3.8×10^{-3} m^2. The test membrane of about 250 µm thickness was sized in a circular shape and an O-ring was used to compress and seal the setup to prevent leaks. Solution containing 100 ppb of lead was forced through the membrane by an externally applied pressure (using a nitrogen cylinder) of 0.4 bar at room temperature to obtain an almost similar flux of 348±25.8 $Lm^{-2}h^{-1}$. The permeate was collected at specific time intervals and analyzed to determine the membrane performance. Upon saturation of the membrane, for re-use tests, the cell was filled with desorption solution (dilute nitric acid solution) and flushed at a flux of 278 $Lm^{-2}h^{-1}$. The regenerated membrane was then washed with deionized water to remove residual desorption solution. The cycle was repeated four times to determine membrane reusability.

Instrumentations

Powered X-ray diffraction analysis was carried out at room temperature on RigakuUltima IV powder diffractometer in Bragg-Brentano geometry, using Cu Kα radiation (λ = 1.5418 A). The 2θ range of 2° to 32° was covered with 0.02° step width and 2°/min scan speed.

ATR-FTIR analyses of the pristine MOF crystals, heavy metal treated MOFs and the nanofibrous MOF membranes were carried out using Agilent tech- Cary 630 (Agilent, Canada) spectrometer carrying a diamond sampling accessory. The samples were pressed on a diamond prism and the infrared spectra were collected at 4 cm^{-1} resolution, 64 scans within a wave number range of 500-3000 cm^{-1} at room temperature.

Transmission electron microscopy (TEM) was carried out to investigate MOF crystal shape and size using a FEI Tecnai F20 apparatus equipped with an Oxford Aztec 80 mm SDD detector. A suspension of the samples prepared in deionised water was dropped on copper grids and analyzed at 300 kV.

Scanning electron microscopy (SEM) images were taken using a Tescan, Vega-II XMU equipped with a 250X EDS, Oxford Inca Energy apparatus. Samples were affixed onto the holder by means of a conductive adhesive, then gold coated under vacuum using an Anatech Hummer VII equipment. Images were taken at suitable resolutions.

Zeta potential and hydrodynamic diameter were recorded using a Zetasizer nano ZS, Malvern instrument. The zeta potential was measured as a function of pH using buffer solutions of different pH. Measurements were carried out using disposable 0.5 mL folded capillary cuvettes and 1 cm length cuvettes for zeta potential and dynamic light scattering measurements, respectively.

The surface elemental composition was determined by X- ray Photoelectron Spectroscopy (XPS, Kratos Axis HS, Manchester, UK). The samples were excited using monochromatized Al K_a X-radiation and a 180^o hemisphere analyzer and a three-channel detector was employed. The samples were analyzed for specific elements at a time in a pressurized chamber ($1.33x10^{-4}$ to $1.33x10^{-5}$ Pa) using an X-ray gun operated at 15 kV and 20 mA. The maximum X-ray penetration depth at $\theta=0^o$ (sample was perpendicular to the detector) was 6.3 nm.

The surface characteristics of the synthesized materials were determined by BET using nitrogen at 77 K with a Micromeritics 3FLEX volumetric apparatus. Before the nitrogen adsorption measurements, the samples were degassed under a purge flow of nitrogen of 40 $cm^3\ min^{-1}$ at 90°C for 1 h. The data in the relative pressure (P/P_0) range 0.05–0.2 were used to calculate the specific surface area with the BET equation.

References

1 Li, Z.-Q., Yang, J.-C., Sui, K.-W. & Yin, N. Facile synthesis of metal-organic framework MOF-808 for arsenic removal. *Mater. Lett.* 2015, **160,** 412–414.

2 Furukawa, H. Gándara, F., Zhang, Y.-B., Jiang, J., Queen, W. L., Hudson, M. R. & Yaghi, O. M. Water adsorption in porous metal-organic frameworks and related materials. *J. Am. Chem. Soc.* 2014, **136,** 4369–4381.

3 Fryxell, G. E. Lin, Y., Fiskum, S., Birnbaum, J. C., Wu, H., Kemner, K. & Kelly, S. Actinide sequestration using self-assembled monolayers on mesoporous supports. *Environ. Sci. Technol.* 2005, **39,** 1324–1331.

4 Lagergren, S. About the theory of so-called adsorption of soluble substances. *K. Sven. vetenskapsakademiens* 1898, **24,** 1–39.

5 Weber, W.J; Morris, J. C. Advances in water pollution research: removal of biologically resistant pollutant from waste water by adsorption. in *International Conference on Water Pollution Symposium* 231–266 (Vol. 2. Pergamon, Oxford, 1962).

6 N. Yin, K. Wang, Y. Xia, Z. Li, Novel melamine modified metal-organic frameworks for remarkably high removal of heavy metal Pb (II). *Desalination* 2012, **430**, 120–127.

7 Q. Yang, Q. Zhao, S. S. Ren, Q. Lu, Guo, Z. Chen, Fabrication of core-shell Fe_3O_4@MIL-100(Fe) magnetic microspheres for the removal of Cr(VI) in aqueous solution. *J. Solid State Chem.* 2016, **244**, 25–30.

8 N. D. Shooto, C. W. Dikio, D. Wankasi, L. M. Sikhwivhilu, F. M. Mtunzi, E. D. Dikio, Novel PVA/MOF Nanofibres: Fabrication, Evaluation and Adsorption of Lead Ions from Aqueous Solution. *Nanoscale Res. Lett.* 2016, **11**, 414 (13 pp).

9 N. D. Shooyo, D. Wankasi, L. M. Sikhwivhilu, E. D. Dikio, Modified Electro-spun Polyvinyl Alcohol Nanofibers Used as Super Adsorbing Material for Lead Ions in Aqueous Solution. *J. Residuals Sci. Tech.* 2016, **13**, 233–242.

10 N. Yin, K. Wang, L. Wang, Z. Li, Amino-functionalized MOFs combining ceramic membrane ultrafiltration for Pb (II) removal. *Chem. Eng. J.* 2016, **306**, 619–628.

11 F. Zou, R. Yu, R. Li, W. Li, Microwave-Assisted Synthesis of HKUST-1 and Functionalized HKUST-1-@$H_3PW_{12}O_{40}$: Selective Adsorption of Heavy Metal Ions in Water Analyzed with Synchrotron Radiation. *ChemPhysChem* 2013, **14**, 2825–2832.

12 F. Ke, J. Jiang, Y. Li, J. Liang, X. Wan, S. Ko, Highly selective removal of Hg^{2+} and Pb^{2+} by thiol-functionalized Fe_3O_4@metal-organic framework core-shell magnetic microspheres. *Appl. Surf. Sci.* 2017, **413**, 266–274.

13 H. Saleem, U. Rafique, R. P. Davies, Investigations on post-synthetically modified UiO-66-NH_2 for the adsorptive removal of heavy metal ions from aqueous solution. *Microporous Mesoporous Mater.* 2016, **221**, 238–244.

14 L. Wang, X. Zhao, J. Zhang, Z. Xiong, Selective adsorption of Pb (II) over the zinc-based MOFs in aqueous solution-kinetics, isotherms, and the ion exchange mechanism. *Environ. Sci. Pollut. Res.* 2017, **24**, 14198–14206.

15 H. Li, H. Liu, J. Zhang, Y. Cheng, C. Zhang, X. Fei, Y. Xian, Platinum Nanoparticle Encapsulated Metal−Organic Frameworks for Colorimetric Measurement and Facile Removal of Mercury (II). *ACS Appl. Mater. Interfaces* 2017, **9**, 40716–40725.

16 X. Luo, T. Shen, L. Ding, W. Zhong, J. Luo, S. Luo, Novel thymine-functionalized MIL-101 prepared by post-synthesis and enhanced removal of Hg(2+) from water. *J. Hazard. Mater.* 2016, **306**, 313–322.

17 Q.-R. Fang, D.-Q. Yuan, J. Sculley, J.-R. Li, Z.-B. Han, H.-C. Zhou, Functional Mesoporous Metal−Organic Frameworks for the Capture of Heavy Metal Ions and Size-Selective Catalysis. *Inorg. Chem.* 2010, **49**, 11637–11642.

18 L. Liang, Q. Chen, F. Jiang, D. Yuan, J. Qian, G. Lv, H. Xue, L. Liu, H.-L. Jiang, M. Hong, *In situ* large-scale construction of sulfur-functionalized metal–organic framework and its efficient removal of Hg(II) from water. *J. Mater. Chem. A* 2016, **4**, 15370–15374.

19 F. Luo, J. L. Chen, L. L. Dang, W. N. Zhou, H. L. Lin, J. Q. Li, S. J. Liu, M. B. Luo, High-performance Hg^{2+} removal from ultra-low-concentration aqueous solution using both acylamide- and hydroxyl-functionalized metal–organic framework. *J. Mater. Chem. A* 2015, **3**, 9616–9620.

20 Y. Y. Xiong, J. Q. Li, L. L. Gong, X. F. Feng, L. N. Meng, L. Zhang, P. P. Meng, M. B. Luo, F. Luo, Using MOF-74 for Hg^{2+} removal from ultra-low concentration aqueous solution. *J. Solid State Chem.* 2016, **246**, 16–22.

21 S. Bhattacharjee, Y.-R. Lee, W.-S. Ahn, Post-synthesis functionalization of a zeolitic imidazolate structure ZIF-90: a study on removal of Hg(II) from water and epoxidation of alkenes. *CrystEngComm* 2015, **17**, 2575–2582.

List of Figures

Figure S1. PXRD analysis of the MOF crystals and when immersed in water 11
Figure S2. N_2 isotherm plot for F300 and MOF 808 12
Figure S3. TEM images of F300 and MOF 808 13
Figure S4. SEM images of the MOF crystals, F300 and MOF 808.....14
Figure S5A. SEM images of PAN nanofibers. PAN without MOF (PAN), PAN with F300 (PA300) and PAN with MOF 808 (PA808). 15
Figure S5B. SEM images of PVDF-MOF nanofibers. PV300 refers to PVDF with F300 incorporated and PV808 refers to PVDF with MOF 808 incorporated.....15
Figure S6. Thermogravimetric analysis (TGA) curves for the MOF crystals (F300 and MOF 808) and the NMOM. PV is PVDF and PA is PAN and the number denotes the MOF particle incorporated e.g. PA300 is PAN with F300 incorporated while PV808 is PVDF with MOF 808 incorporated. 17
Figure S7. The change in pH against the amount of Pb ion removed.....18
Figure S8. X-ray photoelectron spectra (XPS) of the pristine MOFs and the MOF after treatment with heavy metal ion. The similarity of the spectra reveals that the heavy metal ions where not present at surface but inside of the MOF (internal pores). 19
Figure S9A. (a) Cross-sectional view of PA300 after filtration experiments, and (b) elemental EDX mapping of the. PA300 after filtration experiments. 20
Figure S9B. (a) EDX elemental mapping of the top PA 300 layer and bottom PVDF layer, (b) red color represents the Fe mapping of the PA 300 and (b) green color represents the fluorine of the PVDF. 21
Figure S10. FTIR spectra of MOF crystal before and after heavy metal adsorption: (a) F 300 and (b) MOF 808. 22
Figure S11. Sorption data for Pb and the two MOFs when the pH of the system is not adjusted. The shape of the curve is accounted for by the competitive binding of protons and Pb ions.....23
Figure S12. (A) Sorption kinetic data of the MOFs with Pb and Hg ions, (B) Analysis using pseudo-first order, (C) Pseudo-second order model[4], and (D) Morris-webber[5] intraparticle model showing that the sorption is a multistage process and that intraparticle diffusion is not the dominant mechanism. 24

Figure S13. Linearized sorption data for Hg as fitted by (A) Langmuir, (B) Freundlich, and (C) Temkin Isotherm models 25
Figure S14. Linearized sorption models for Pb: (A) Langmiur Isotherm, (B) Freundlich Isotherm, and (C) Temkin Isotherm models. 26

List of Tables

Table S1. Kinetic model parameters for all three models with the two MOFs. ……..26
Table S2. Langmuir model parameters for sorption of Pb(II). ……...….26
Table S3. Freundlich model parameters for sorption of Pb(II). ……26
Table S4. Temkin model parameters for Pb(II) sorption. ……26
Table S5. Langmuir model parameters for sorption of Hg(II). ……26
Table S6. Freundlich model parameters for sorption of Hg(II). ……26
Table S7. Temkin model parameters for Hg(II) sorption. ……30
Table S8. The adsorption capacity, source of metal ion, pH, and time to adsorption equilibrium of Pb and Hg. 26

Characterization:

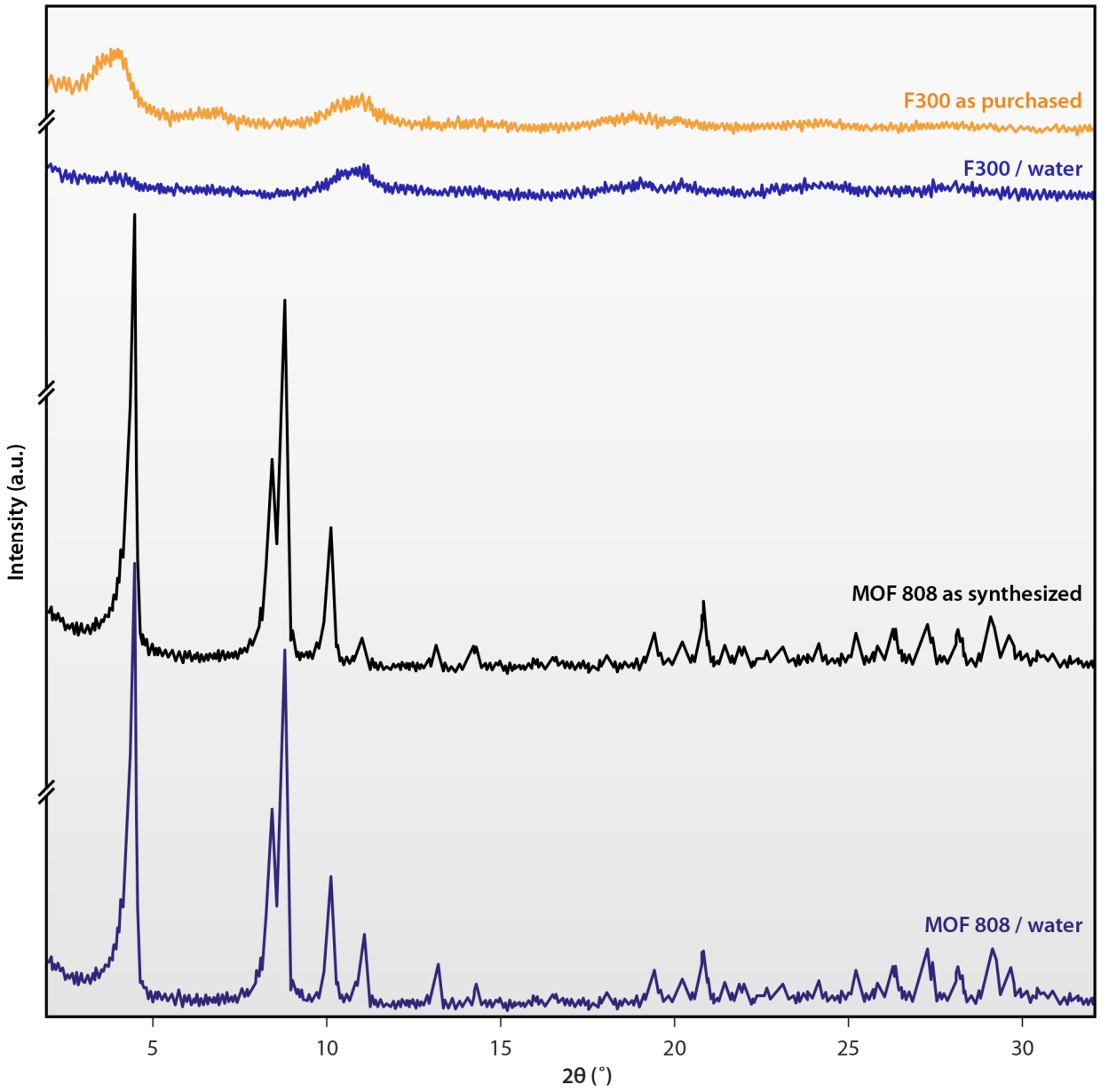

Figure S1. PXRD analysis of the MOF crystals and when immersed in water.

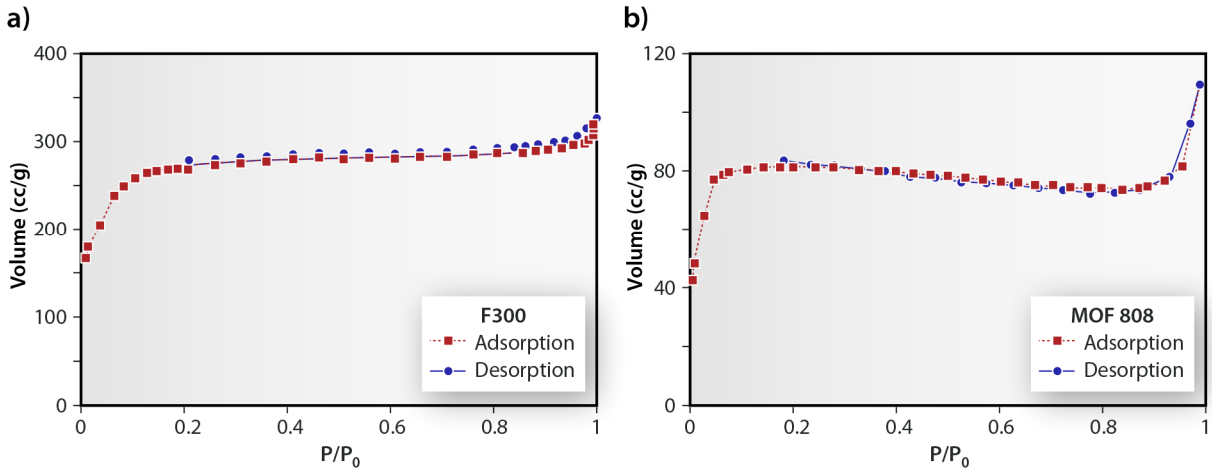

Figure S2. N_2 isotherm plot for M808 and F300.

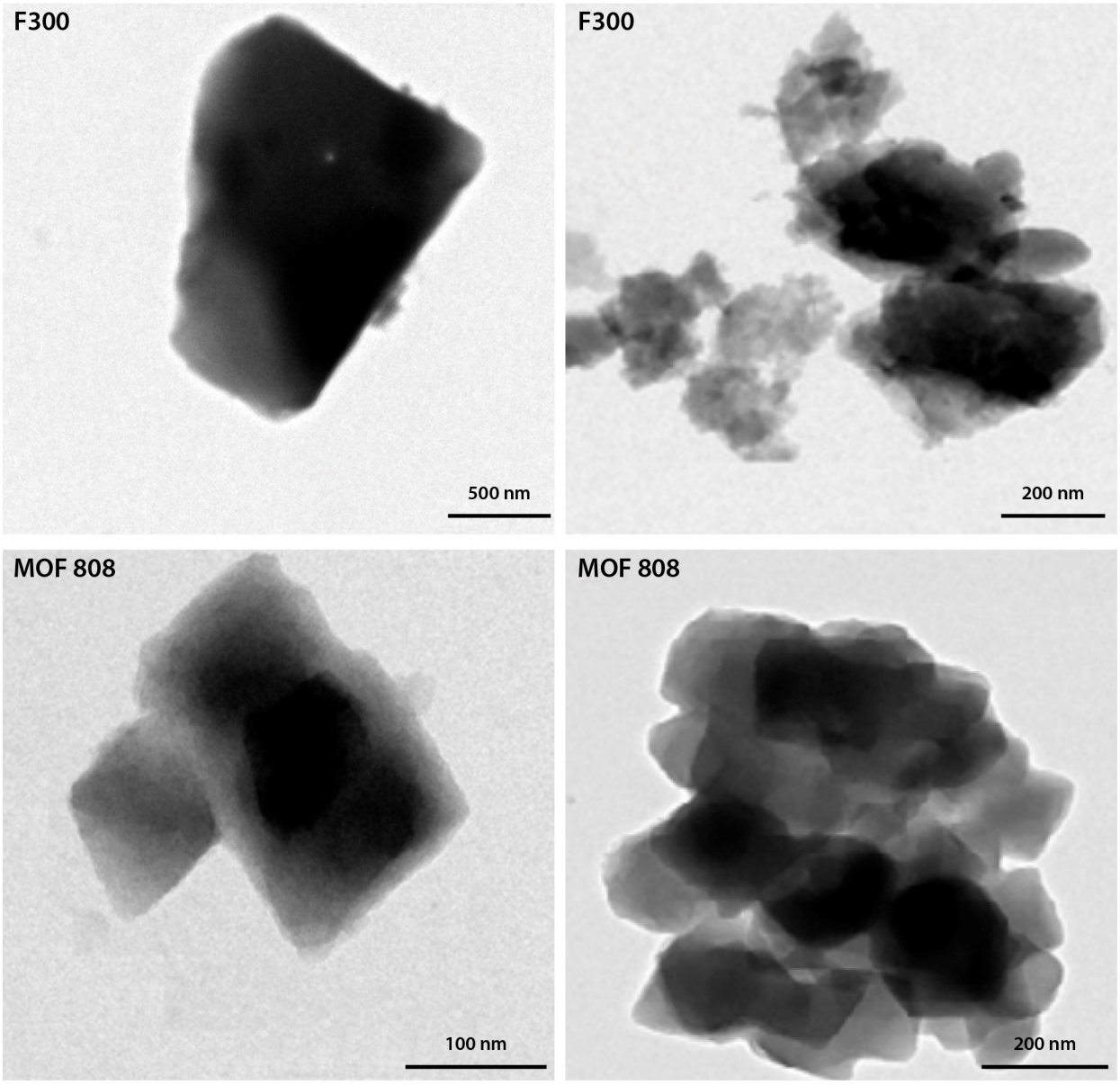

Figure S3. TEM images of M808 and F300.

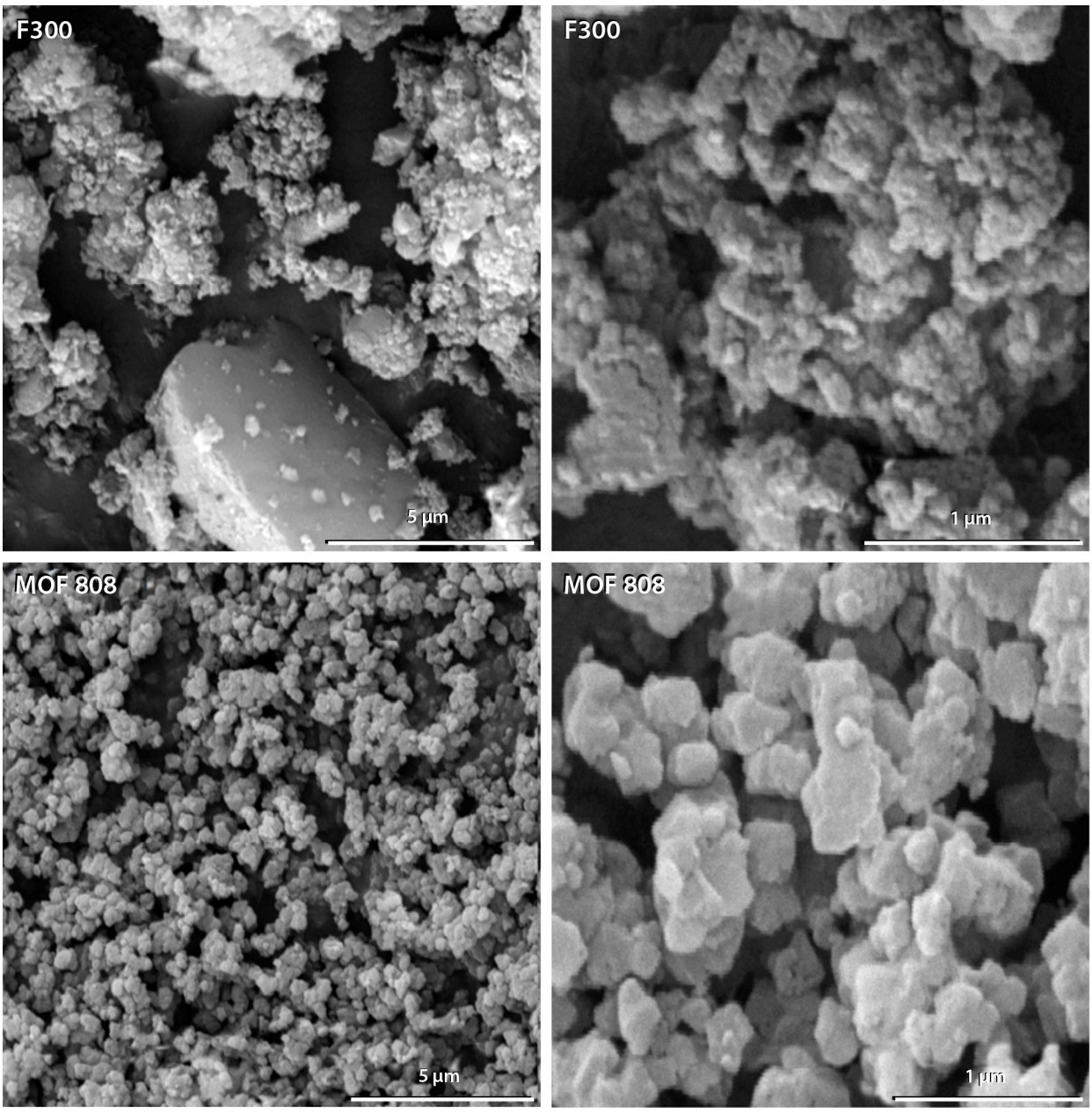

Figure S4. SEM images of the MOF crystals, M808 and F300.

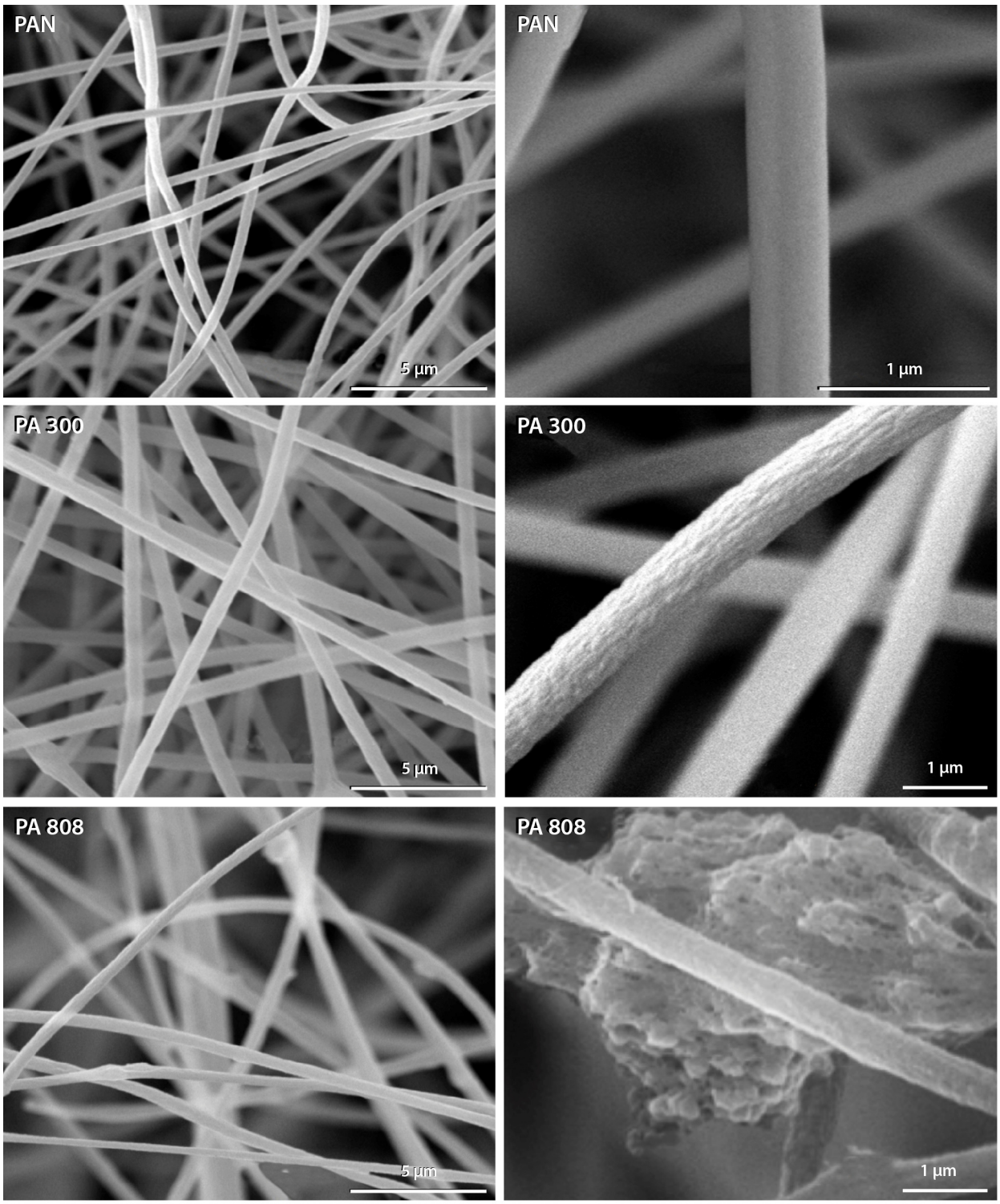

Figure S5A. SEM images of PAN nanofibers. PAN without MOF (PAN), PAN with F300 (PA300) and PAN with MOF 808 (PA808).

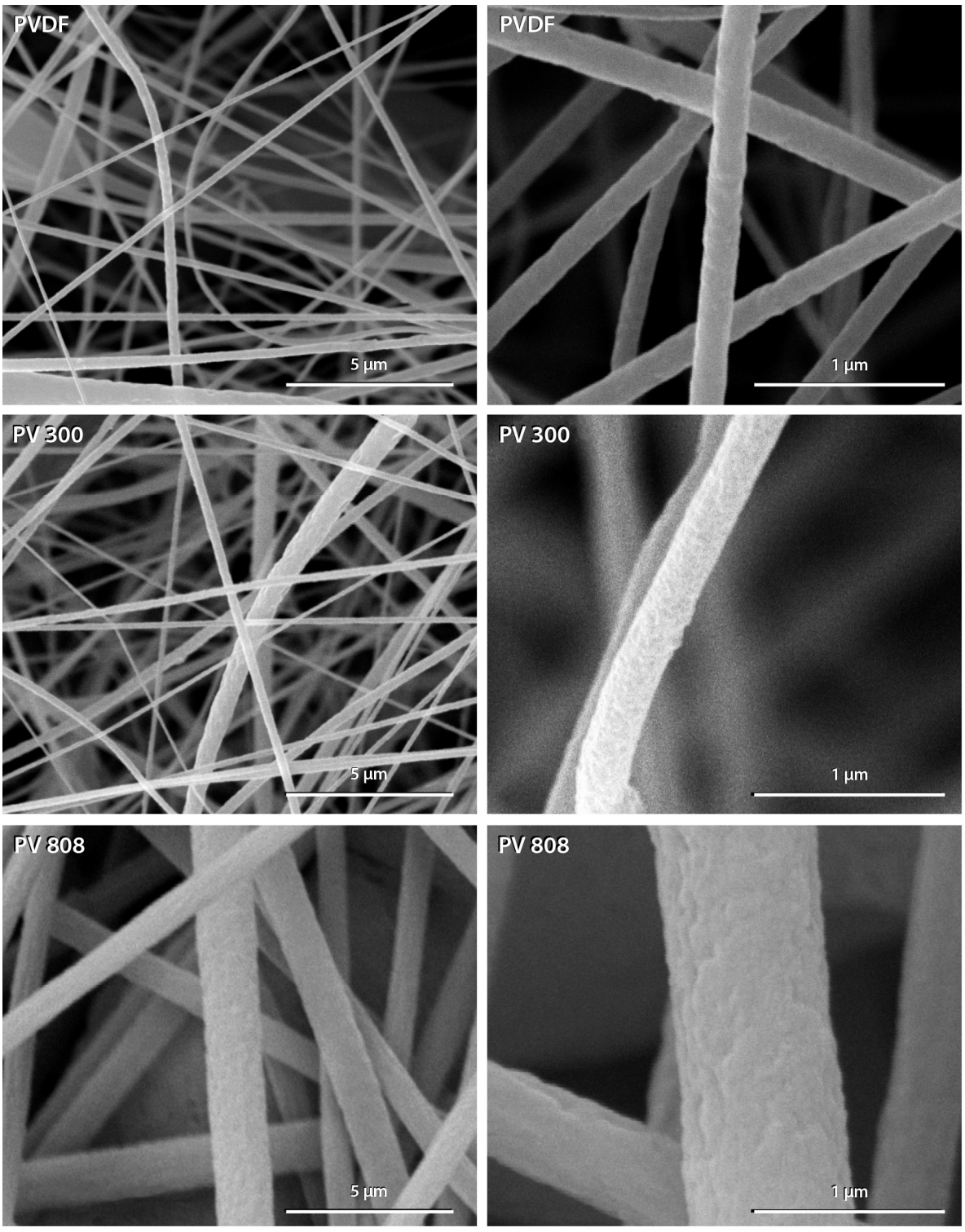

Figure S5B. SEM images of PVDF-MOF nanofibers. PV300 refers to PVDF with F300 incorporated and PV808 refers to PVDF with M808 incorporated.

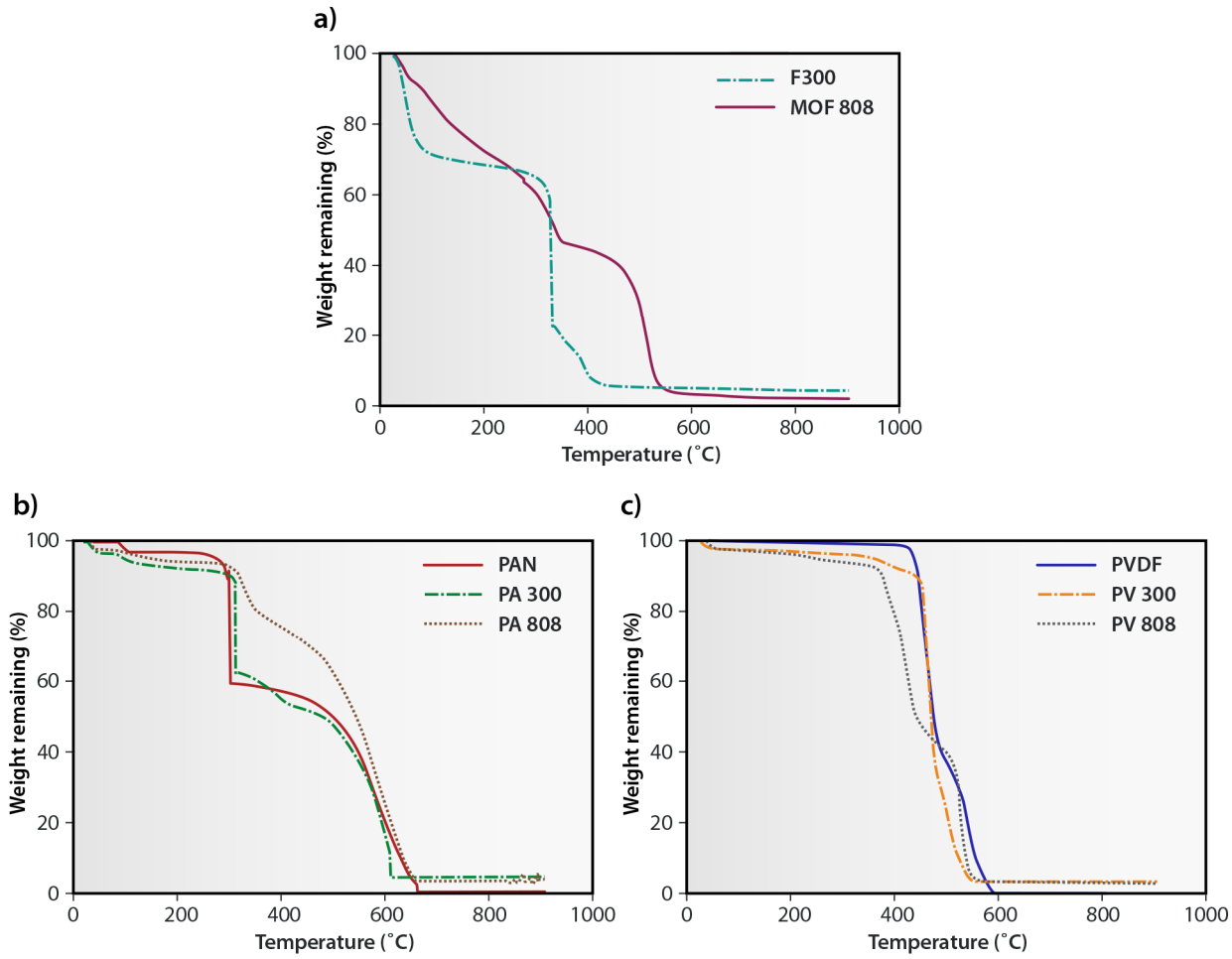

Figure S6. Thermogravimetric analysis (TGA) curves for the MOF crystals (M808 and F300) and the NMOM. PV is PVDF and PA is PAN and the number denotes the MOF particle incorporated e.g. PA300 is PAN with F300 incorporated while PV808 is PVDF with MOF 808 incorporated.

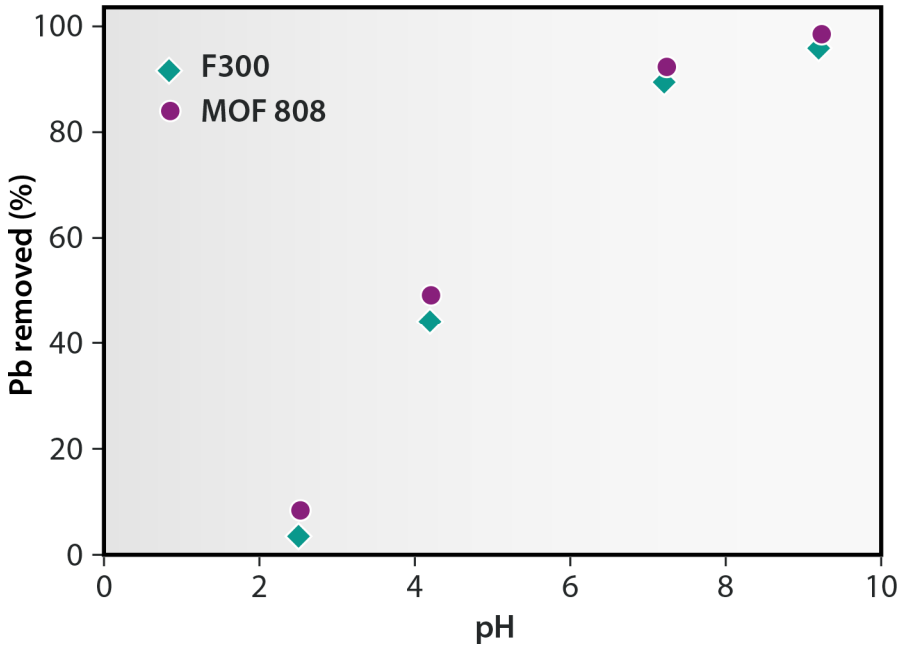

Figure S7. The change in pH against the amount of Pb ion removed.

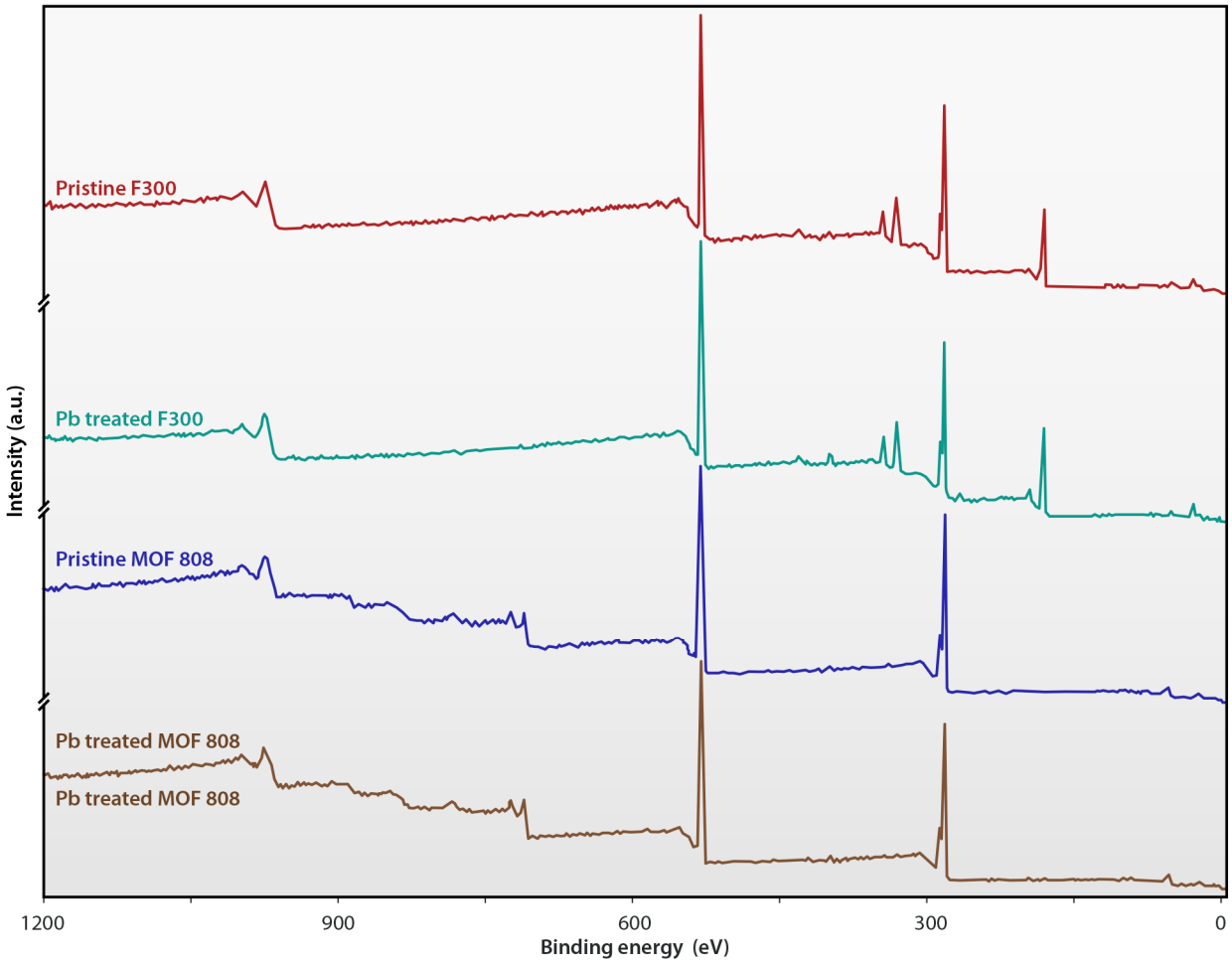

Figure S8. X-ray photoelectron spectra (XPS) of the pristine MOFs and the MOF after treatment with heavy metal ion. The similarity of the spectra reveals that the heavy metal ions were not present at surface but inside of the MOF (internal pores).

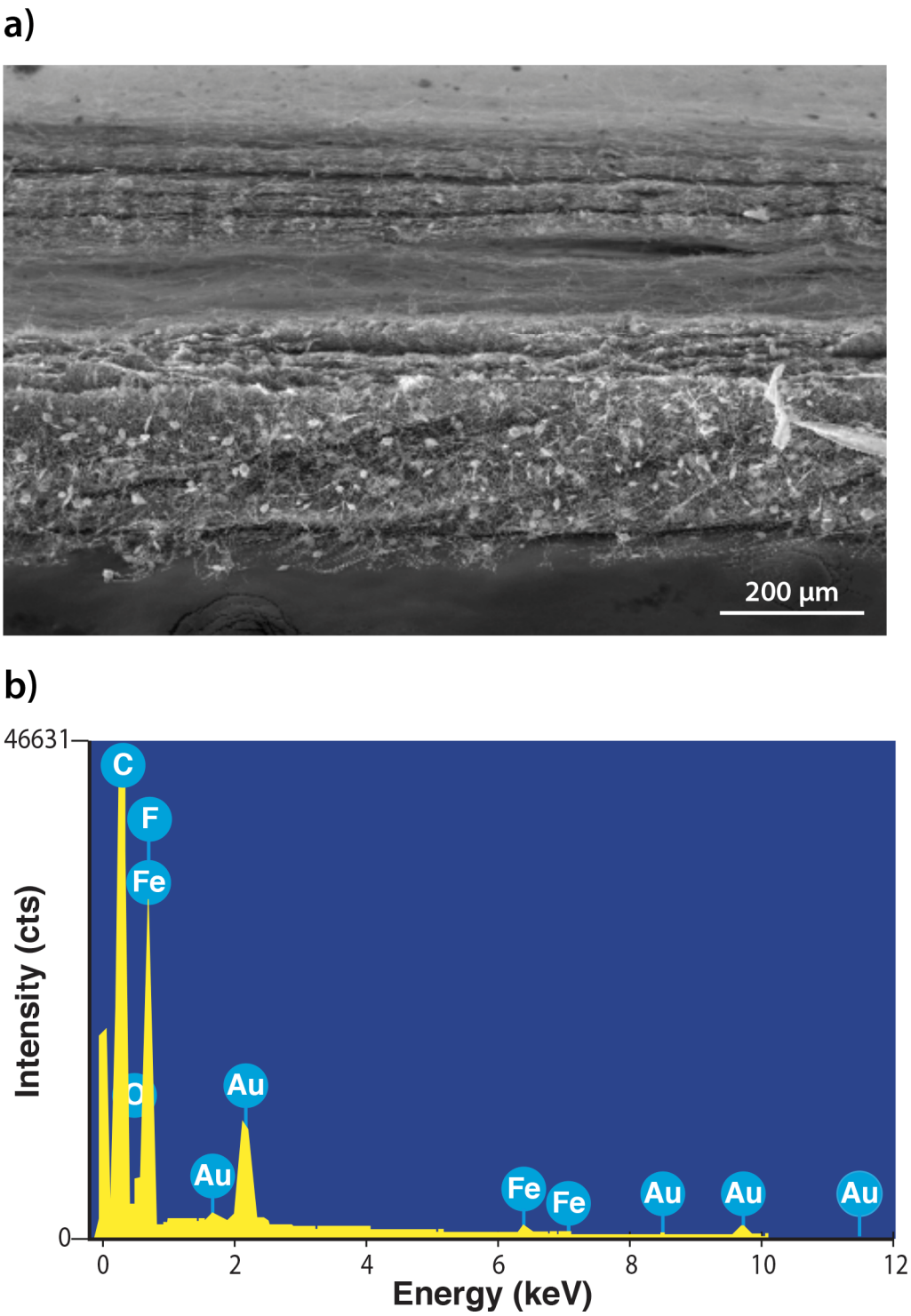

Figure S9A. Elemental EDX mapping of the cross-sectional view of PA300 after filtration experiments.

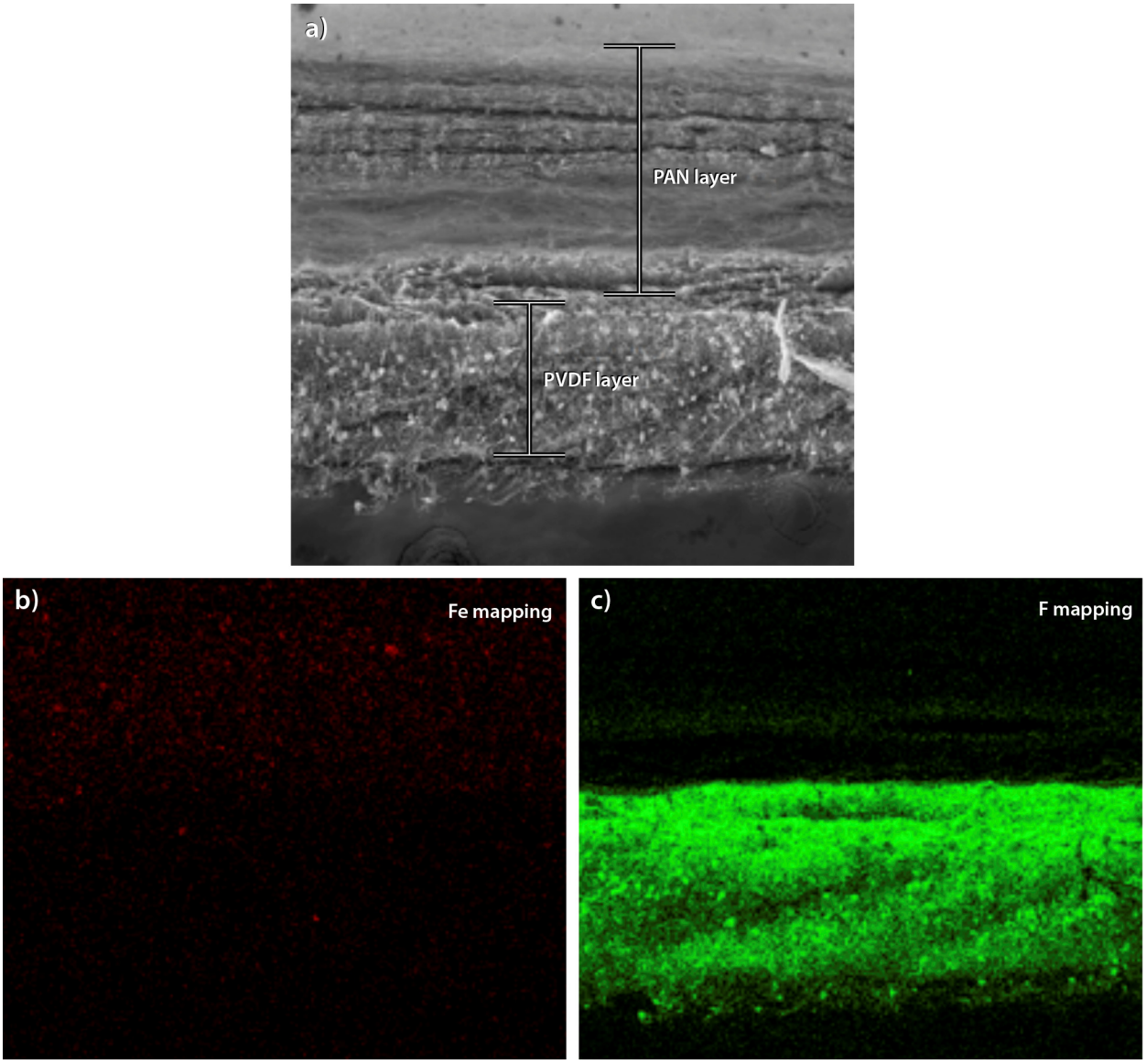

Figure S9B. EDX elemental mapping of the lower PVDF layer and top PAN300 layer. The green color represents the Fluoride ion of the PVDF and Fe ions of the F300.

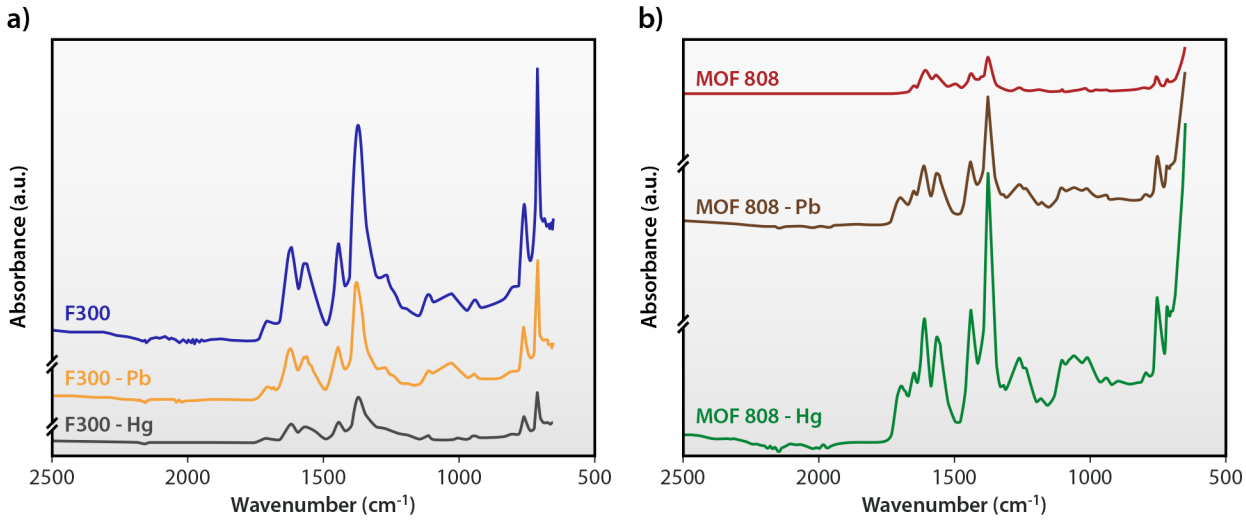

Figure S10. FTIR spectra of MOF crystal before and after heavy metal adsorption.

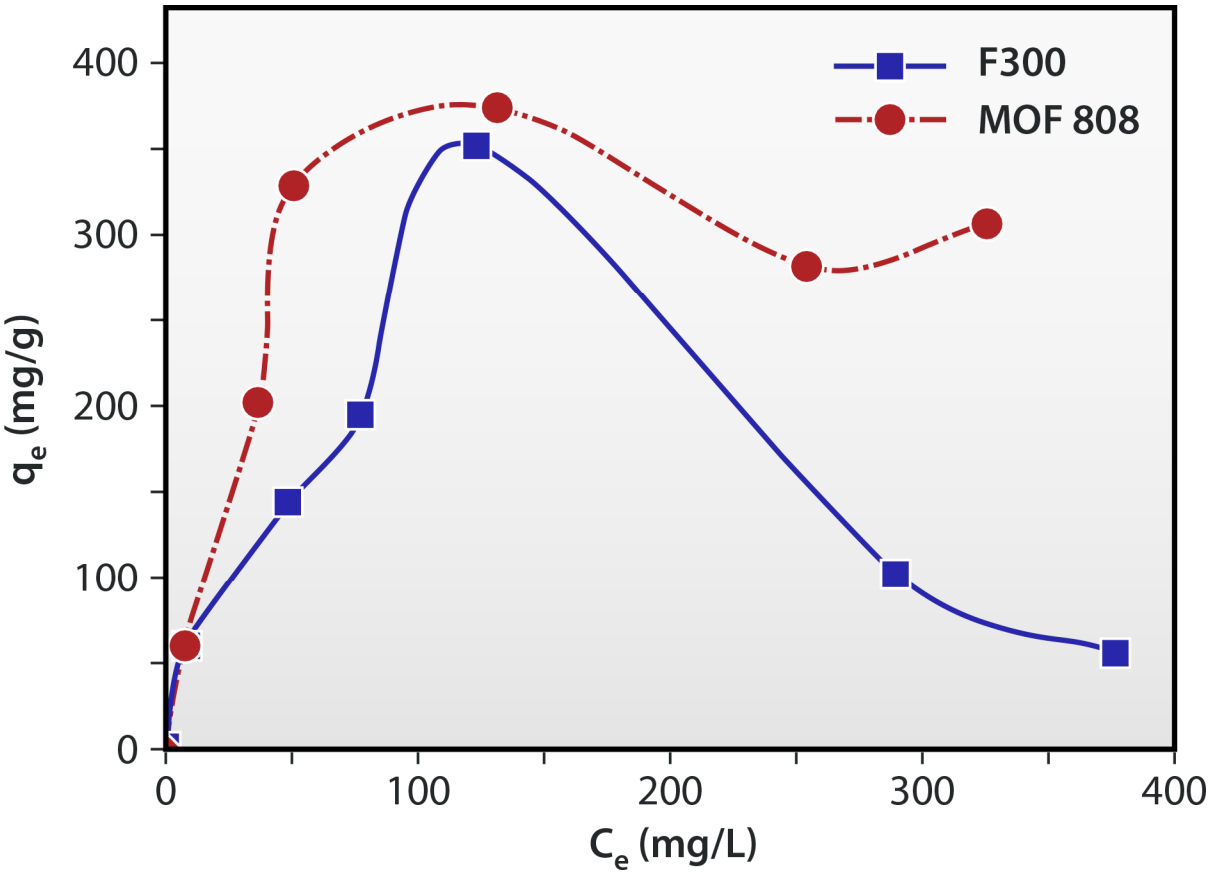

Figure S11. Sorption data for Pb and the two MOFs when the pH of the system is not adjusted. The shape of the curve is accounted for by the competitive binding of protons and Pb ions.

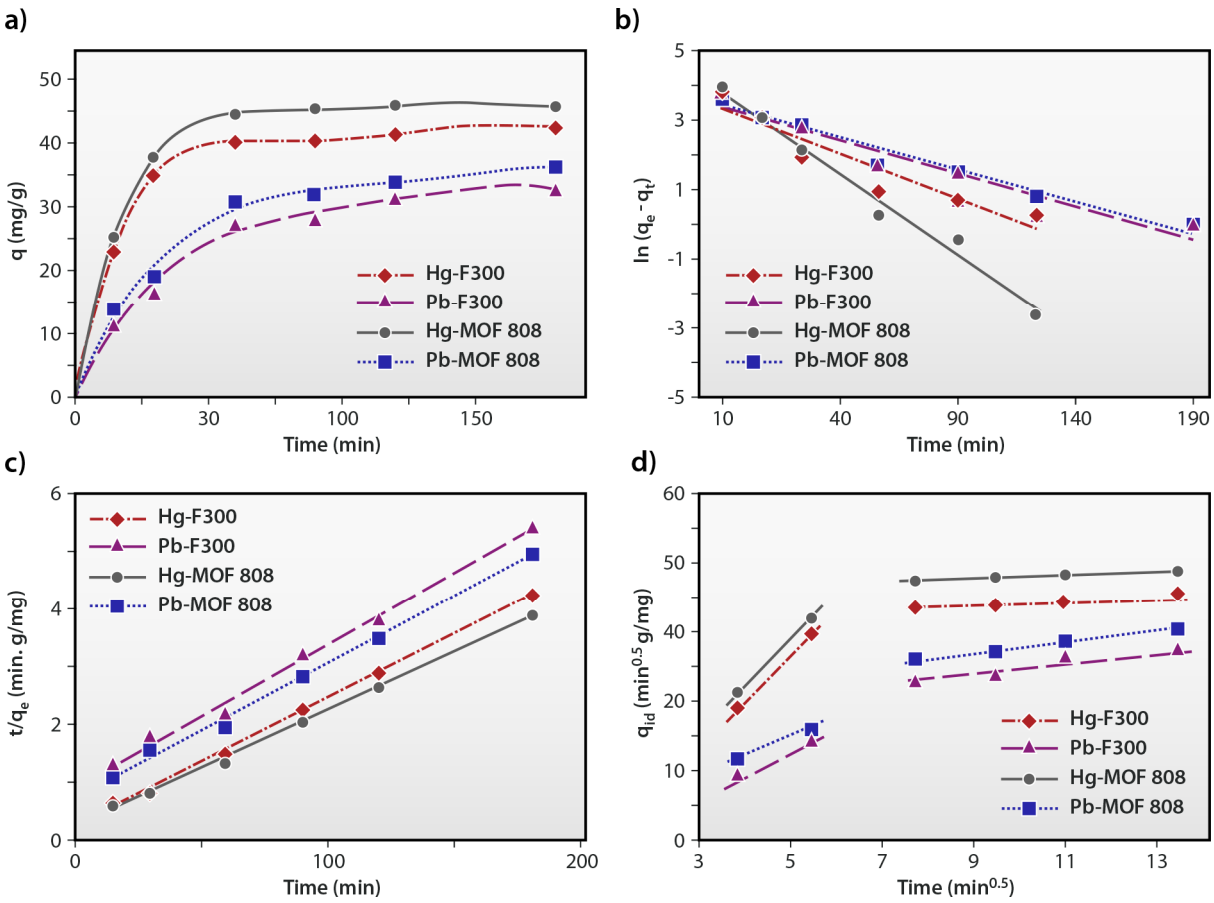

Figure S12. (A) Sorption kinetic data of the MOFs with Pb and Hg ions, (B) Analysis using pseudo-first order, (C) Pseudo-second order model[4], and (D) Morris-Webber[5] intra-particle model showing that the sorption is a multistage process and that intra-particle diffusion is not the dominant mechanism.

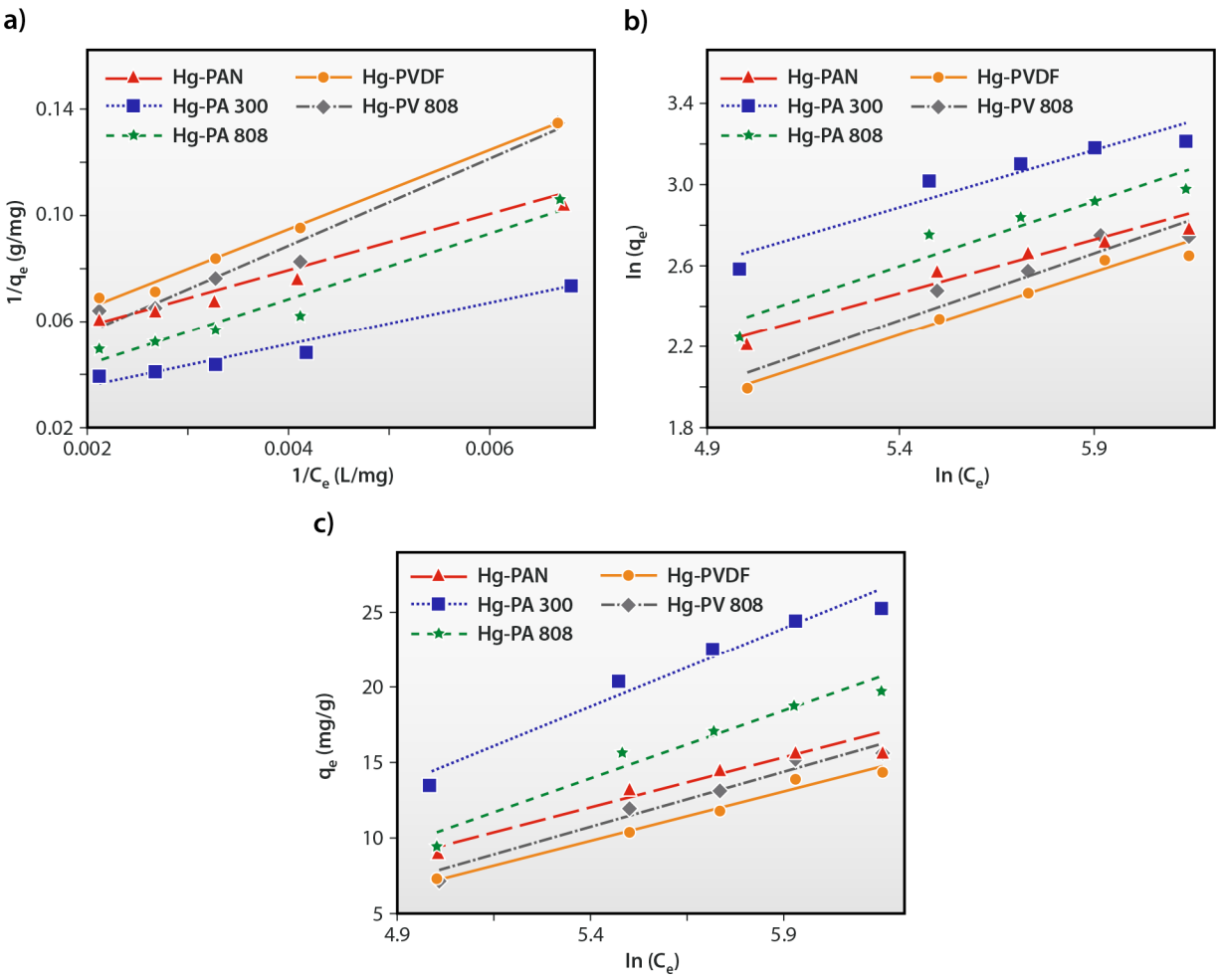

Figure S13. Linearized sorption data for Hg as fitted by (A) Langmuir, (B) Freundlich, and (C) Temkin Isotherms.

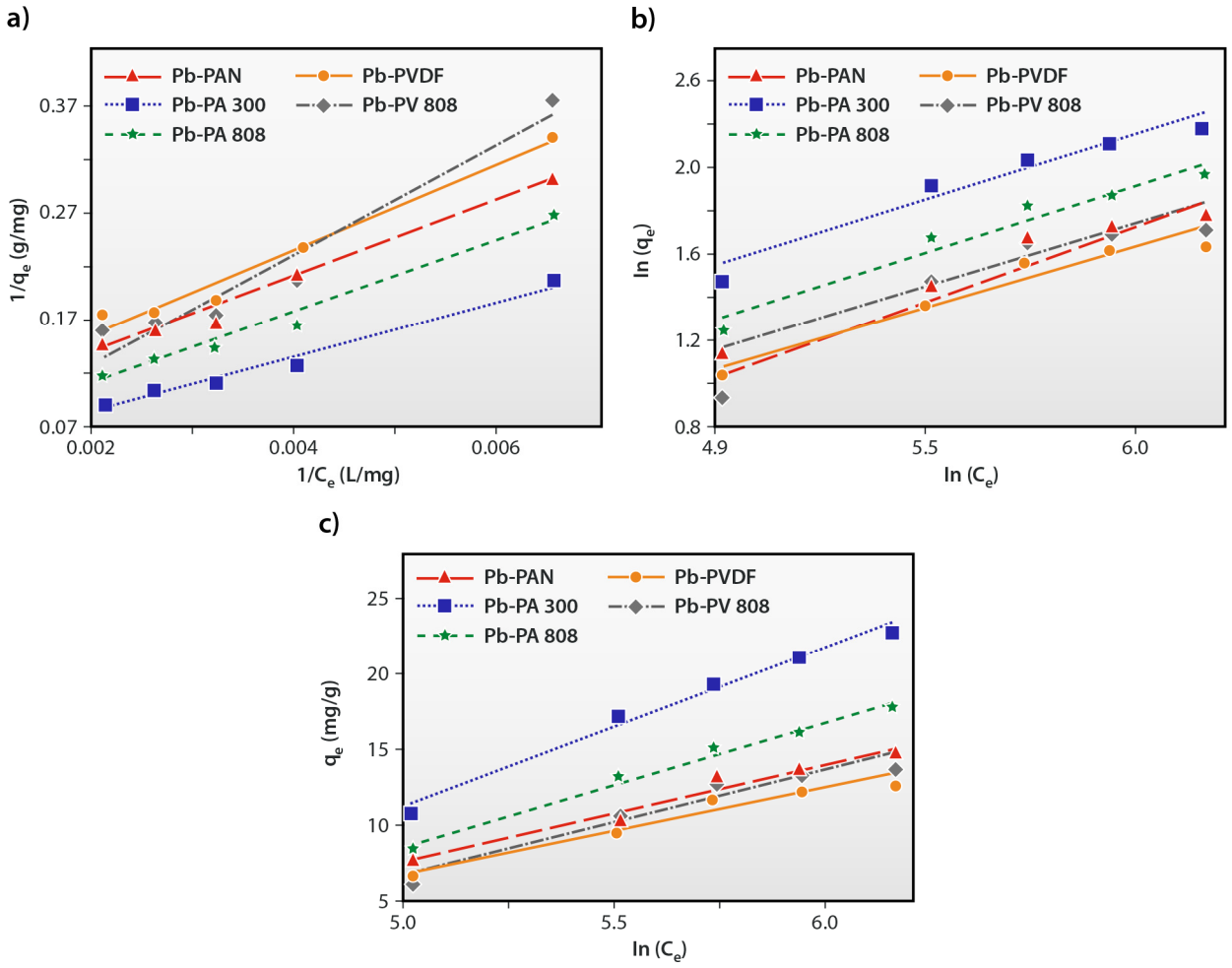

Figure S14. Linearized sorption models for Pb: (A) Langmiur Isotherm, (B) Freundlich Isotherm, and (C) Temkin Isotherm models.

Table S1. Kinetic model parameters for all three models with the two MOFs.

		First order			Second order			Intra-particle	
Adsorbate	**Sorbent**	k_1	q_e	R^2	k_2	q_e	R^2	k_{id}	R^2
Pb(II)	F300	0.025	32.237	0.971	0.880	40.013	0.994	2.610	0.942
	M808	0.023	32.256	0.969	0.723	43.130	0.994	2.843	0.934
Hg(II)	F300	0.028	25.908	0.894	0.234	45.436	0.998	3.071	0.798
	M808	0.052	42.423	0.987	0.196	49.328	0.997	3.386	0.795

k_1, k_2 [min^{-1}], k_{id} [$mg/g/min^{-1}$], q_e [$mg\ g^{-1}$]

Table S2. Langmuir model parameters for sorption of Pb(II).

Sorbent	q_{max} **(mg** g^{-1}**)**	K_L (L mg^{-1})	R^2	K_d (mL g^{-1})
F300	148.133	0.014	0.995	2.7×10^4
M808	170.740	0.014	0.970	1.3×10^4
PAN	15.097	0.002	0.983	8.1×10^3
PA808	23.977	0.001	0.980	1.1×10^4
PA300	30.193	0.001	0.976	1.4×10^4
PVDF	13.621	0.002	0.975	6.0×10^3
PV300	NA[⊥]	NA	NA	NA
PV808	17.191	0.0001	0.945	9.3×10^3

[⊥]NA means Not Available

Table S3. Freundlich model parameters for sorption of Pb(II).

Sorbent	k ($(mg\,g^{-1}(L/mg)^{1/n}$)	n	R^2
F300	12.181	2.555	0.933
M808	10.471	2.231	0.961
PAN	0.130	1.541	0.956
PA300	0.159	1.442	0.947
PA808	0.056	1.274	0.890
PVDF	0.122	1.566	0.934
PV300	NA	NA	NA
PV808	0.056	1.274	0.890

Table S4. Temkin model parameters for Pb(II) sorption.

Sorbent	B	A_T (L g^{-1})	b_T (J mol^{-1})	R^2
F300	30.512	0.027	81.201	0.970
M808	40.874	0.027	60.614	0.956
PAN	3.085	0.019	802.981	0.968
PA300	5.056	0.018	490.032	0.984
PA808	3.966	0.017	624.689	0.989
PVDF	2.669	0.020	928.215	0.952
PV300	NA	NA	NA	NA
PV808	3.302	0.016	750.349	0.927

Table S5. Langmuir model parameters for sorption of Hg(II).

Sorbent	q_{max} **(mg g^{-1})**	K_L (L mg^{-1})	K_d (mL g^{-1})	R_L	R^2
F300	229.659	0.003	3.1 x 10^4	0.373	0.992
M808	276.960	0.002	3.9 x 10^4	0.374	0.995
PAN	28.767	0.003	9.4 x 10^3	0.478	0.987
PA808	53.088	0.002	2.3 x 10^4	0.481	0.951
PA300	50.889	0.003	3.1 x 10^4	0.470	0.965
PVDF	28.640	0.002	5.2 x 10^3	0.484	0.994
PV300	NA	NA	NA	NA	NA
PV808	42.603	0.001	8.3 x 10^3	0.485	0.971

Table S6. Freundlich model parameters for sorption of Hg(II).

Sorbent	k $((mg\,g^{-1}(L_f/mg)^{1/n})$	**n**	R^2
F300	4.261	1.841	0.905
M808	2.490	1.519	0.978
PAN	0.693	1.908	0.958
PA300	0.868	1.780	0.917
PA808	0.400	1.540	0.904
PVDF	0.352	1.632	0.978
PV300	NA	NA	NA
PV808	0.269	1.483	0.936

Table S7. Temkin model parameters for Hg(II) sorption.

Sorbent	**B**	**A_T (L g^{-1})**	**b_T (J mol^{-1})**	**R^2**
F300	40.357	0.049	61.391	0.968
M808	60.858	0.027	40.711	0.961
PAN	6.533	0.028	379.249	0.984
PA300	10.544	0.026	234.977	0.951
PA808	9.100	0.021	272.269	0.947
PVDF	6.496	0.021	381.389	0.981
PV300	NA	NA	NA	NA
PV808	7.475	0.019	331.461	0.966

Table S8. The adsorption capacity, source of metal ion, pH, and time to adsorption equilibrium of Pb and Hg.

Metal ion	Sorbent	Adsorption capacity [mg g^{-1}]	Metal ion source	pH	Time to adsorption equilibrium [min]	Reference
Pb	Melamine-Zr-MOFs	122	$Pb(NO_3)_2$	5	120	6
	Fe_3O_4@$Cu_3(BTC)_2$	215.05	$Pb(NO_3)_2$	6	120	7
	PVA nanofiber/La-TBC	184	$Pb(NO_3)_2$	-	10	8
	PVA/Co-MOF	49.64		5.03	30	9
	Cu-terepthalate MOF	80	$Pb(NO_3)_2$	7	120	10
	HKUST-1-MW@$H_3PW_{12}O_{40}$	98		7	10	11
	UiO-66-NHC(S)NHMe	232	¶NA	-	240	12
	TMU-5	251	NA	10	15	13
	MOF 800	170.74	$Pb(NO_3)_2$	5	50	This study
	PA808	119.9	$Pb(NO_3)_2$	5	90	This study
	PV808	85.95	$Pb(NO_3)_2$	5	90	This study
	F300	148.13	$Pb(NO_3)_2$	5	50	This study
	PA300	150.95	$Pb(NO_3)_2$	5	90	This study
Hg	Pt NP@UiO-66-NH_2	206.25	$HgCl_2$	5	30	14
	ZIF-90-SH	22	$HgCl_2$	-	1440	15
	MIL-101-Thymine	52	$HgCl_2$	6	200	16
	AMOF-1	78	NA	-	1440	16
	Fe_3O_4@SiO_2@HKUST-1	264	$HgCl_2$	3	10	18
	Zn(hip)(L)(DMF)(H_2O)	333	$Hg(NO_3)_2$	5	60	19
	SH@SiO_2/$Cu(BTC)_2$	210	NA	5.5	60	20
	MOF-74-Zn	63	$Hg(NO_3)_2$	6	90	21
	MOF 800	276.96	$HgCl_2$	5	50	This study
	PA808	254.4	$HgCl_2$	5	90	This study
	PV808	213	$HgCl_2$	5	90	This study
	F300	229.66	$HgCl_2$	5	50	This study
	PA300	265.45	$HgCl_2$	5	90	This study

¶ NA means Not Available

Author Information:

Correspondence and requests for materials should be addressed to Dipak Rana (rana@uottawa.ca).